National Institute of Standards and Technology high-accuracy cryogenic radiometer

T. R. Gentile, J. M. Houston, J. E. Hardis, C. L. Cromer, and A. C. Parr

A high-accuracy cryogenic radiometer has been developed at the National Institute of Standards and Technology to serve as a primary standard for optical power measurements. This instrument is an electrical-substitution radiometer that can be operated at cryogenic temperatures to achieve a relative standard uncertainty of 0.021% at an optical power level of 0.8 mW. The construction and operation of the high-accuracy cryogenic radiometer and the uncertainties in optical power measurements are detailed.

Key words: Radiometry, cryogenic, National Institute of Standards and Technology, standards, electrical substitution.

1. Introduction

Until recently, the primary standard for optical power measurements at the National Institute of Standards and Technology (NIST) was a silicon photodiode-based device with nearly 100% quantum efficiency.[1] This device consists of three inversion-layer photodiodes in a light-trapping arrangement, and the relative standard uncertainty in its quantum efficiency is 0.11%.[2] Although this device provides a convenient standard, it is currently the limiting element in the accuracy of several NIST radiometric scales such as detector spectral response[2] and the detector realization of the candela.[3] Furthermore, for applications requiring the highest accuracy, its spectral range is limited to 450–700 nm. To obtain improved accuracy and increased spectral range of the primary standard, we have developed a high-accuracy cryogenic radiometer (HACR), which is an electrical-substitution device that can be operated near the temperature of liquid helium. In a previous paper,[4] measurements of the quantum efficiency of silicon photodiode light-trapping detectors obtained by the use of both the HACR and the NIST Spectral Comparator Facility were compared and found to agree within the combined uncertainties of the measurements. We describe the construction, operation, and accuracy of the HACR in this paper, whereas its use in a new realization of the NIST scale of detector spectral response is described in a companion paper.[5]

An electrical-substitution radiometer can be used to link optical power measurements to the watt by comparing the temperature rise induced in an absorbing mass by incident optical radiation to that induced by electrical heating. (We use the term optical to refer to all electromagnetic radiation from ultraviolet to infrared wavelengths, i.e., wavelengths of roughly 200 nm to 20 μm.) Although this technique is nearly a century old,[6] only recently have these devices been operated at cryogenic temperatures, which allows relative standard uncertainties of 0.01% in measurements of optical power. Cryogenic electrical substitution radiometry was first developed at NIST for temperature measurements,[7] and soon thereafter for the calibration of low-temperature vacuum blackbodies.[8,9] A similar apparatus was also developed at the National Physical Laboratory (NPL) in the United Kingdom in conjunction with Oxford Instruments, first to perform a measurement of the Stefan–Boltzmann constant,[10,11] and shortly thereafter for high-accuracy measurements of optical power that use collimated radiation.[12] The NIST HACR is also based on the NPL–Oxford design. However, changes have been made in the design and operation, especially in the instrumentation and computer control of the measurement process. Furthermore, we have performed an additional analysis of the accuracy of the HACR, as operated at NIST. Another radiometer based on the NPL–Oxford design is in use at the Physikalisch-Technische Bundesanstalt in Berlin, Germany.[13]

The authors are with the National Institute of Standards and Technology, Gaithersburg, Maryland 20899.

Received 27 July 1995; revised manuscript received 16 October 1995.

The organization of the paper is as follows. In Section 2 we describe the radiometer, the accompanying laser system, and the measurement instrumentation. In Section 3 we describe the measurement procedures and analyze the accuracy of the HACR. We conclude the paper and discuss future goals in Section 4.

2. Apparatus

A drawing of the HACR is shown in Fig. 1 and a detailed view of its critical elements is shown in Fig. 2. The essential elements of the HACR are a copper cavity (designed to maximize the absorption of radiation), an electrical heater located on this cavity, a reference block maintained at a fixed temperature, and a weak thermal link between the cavity and the reference block. Optical or electrical heating raises the temperature of the cavity above that of the reference block; a new equilibrium temperature is reached when the heating is balanced by the heat flow through the weak thermal link to the reference block. Heating is first performed with optical power, and then the magnitude of this power is determined by finding the electrical power that yields the same temperature rise.

There are two conflicting requirements for the size of the cavity: A small cavity has a low heat capacity, allowing a short time constant, which is desirable for precise and practical measurements. However, a large cavity with a small entrance aperture maximizes the absorption by reducing the light lost by diffuse reflection from the cavity. A major advantage of operating at a temperature of 5 K is that the heat capacity of copper is reduced from the room-temperature value by a factor of ~1000, which allows a large, highly absorptive cavity to be used without degrading the time constant. Another advantage of low-temperature operation is the dramatically reduced radiative coupling of the cavity to its surroundings. The only thermal radiation from room temperature that reaches the cavity originates at the window and is transmitted through a narrow solid angle defined by the cold shields. Finally, the use of superconducting leads effectively eliminates the lead-heating error in room-temperature electrical-substitution radiometers, which is due to heat generated in the wires to the heater.[6]

Although the time constant of the system is dramatically reduced from several days at room temperature to roughly 4 min at 5 K, it is still longer than desired. To improve the speed and accuracy with which measurements can be obtained, we fit the time dependence of the voltage across the temperature sensor to a mathematical model, so as to predict the asymptotic temperature of the cavity. Furthermore, we have automated the measurements under computer control, which is essential for the practical use of the HACR as a primary standard and which

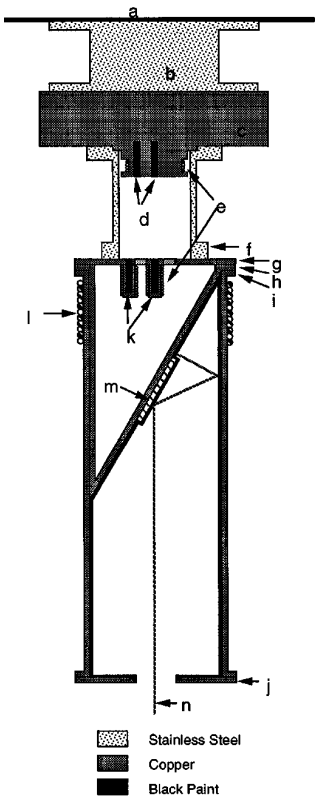

Fig. 2. Detailed view of the critical elements of the HACR: a, liquid-helium reservoir; b, thermal link between liquid-helium reservoir and the reference block; c, reference block (5 K); d, reference-block GRT's; e, thermal anchoring of GRT leads; f, thermal link between the reference block and the cavity; g, top end cap of cavity; h, slanted piece within cavity; i, cavity cylinder; j, bottom end cap of cavity; k, cavity GRT's; l, wire-wound heater; m, thin-film heater; n, laser beam.

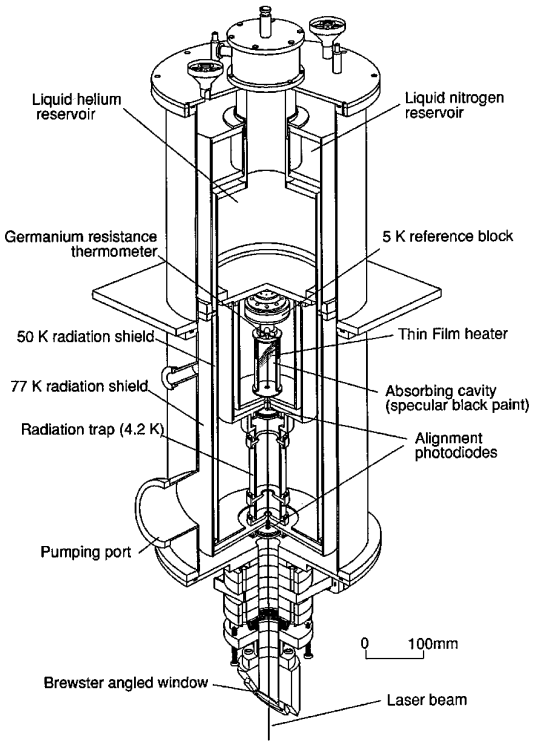

Fig. 1. NIST high-accuracy cryogenic radiometer.

also permits a more thorough evaluation of the measurement uncertainties.

A. Construction of the Radiometer

1. Cryostat

The liquid-helium cryostat shown in Fig. 1 constitutes most of the physical size of the radiometer. A collimated optical beam enters the radiometer through a window at the bottom of the cryostat. Although the electrical-substitution method requires only that the heat load on the cavity from sources other than the applied optical or electrical power be constant, the best first step toward this goal is isolating the cavity from all other heat sources. For heat exchange with the environment to be minimized, the cryostat is maintained at a pressure of less than 10^{-5} Pa (10^{-7} Torr) by a turbomolecular pump and the cryopumping by the liquid-helium and liquid-nitrogen reservoirs. For radiative heating to be minimized, the cavity is nested inside four shields: two 4.2-K shields attached to the liquid-helium reservoir, a shield between the liquid-helium and liquid-nitrogen reservoirs, and a 77-K shield attached to the liquid-nitrogen reservoir. The only break in this shielding is for the path of the optical beam. The effects of thermal radiation along this path are discussed in Subsection 3.D.

2. Reference Block and Thermal Link

The cavity is connected to a copper reference block by a thin-walled stainless-steel tube. In the absence of optical or electrical heating, the cavity temperature is very near the temperature of the reference block. The weak thermal link allows a 1-K rise in the temperature of the cavity with respect to the reference block for an input power to the cavity of 1 mW. The reference block is connected to the liquid-helium reservoir, but its temperature is elevated to 5 K by the use of a wire-wound heater, and it is actively stabilized with a temperature controller.[14,15] There are two germanium resistance thermometers (GRT's) on the reference block; one is used as the input for the control circuitry. A constant current source, external to the temperature controller, is used to supply current to the control GRT. The temperature stability, as determined by monitoring the other thermometer, is typically 150 μK during a typical measurement period of 45 min, and 350 μK over many hours. However, occasional excursions (origin not yet clearly identified) of as much as 350 μK may occur on the time scale of a measurement.

3. Cavity

The receiving cavity is designed for nearly complete absorption of laser radiation. It consists of an electroformed copper cylinder, 15 cm long, 5 cm in diameter, and weighing 220 g. Within the cavity is included a surface that is inclined at a 30° angle to the axis of the cylinder. The interior of the cavity is coated with a specular black paint,[16] except for the inside of the bottom end cap, which is painted with a diffusely reflecting black paint.[17] As shown in Fig. 2, the laser beam enters the cavity through a 12-mm aperture in the bottom end cap and undergoes five specular reflections within the cavity. The absorptance of the cavity was determined to be 99.998% by comparison with a NIST reflectance standard of 632.8 nm. (For an analysis of the absorptance of this cavity design, see Ref. 12.) Datla *et al.*[18] measured the specular and diffuse reflectance of Chemglaze Z302 at an incident angle of 45° to be below 10% and 1%, respectively, over the wavelength range from 0.3 to 40 μm; in the narrower range between 0.4 and 15 μm, the specular reflectance was measured to be between 5% and 7%. Recently Stock and Hofer[19] measured the temperature dependence of the reflectance of a cavity coated with Chemglaze Z302. When it was cooled from 293 K to 4 K, they found a reproducible, reversible decrease of the reflectance of 10%. Because of the low absolute value of the reflectance of the HACR cavity, this change in the reflectance with temperature is a negligible effect for our measurements.

4. Electrical Heaters

A fundamental requirement for the validity of the electrical-substitution method is that the electrical heater should produce the same temperature rise, for an equal applied power, as the optical source. The uncertainty in measuring the optical power because of possible nonequivalence of the two heating methods is discussed in Subsection 3.C. As a way to make the two heating methods as equivalent as possible, a thin-film resistive heater was deposited at the position where the laser beam first strikes the inside of the cavity, before being painted over with Chemglaze. The heater consists of a resistive layer (1-cm-diameter, 0.1-mm-thick carbon-loaded polymer) and electrical contacts (0.1-mm-thick silver-loaded polymer), deposited over two insulating layers (2.5 cm diameter, each 0.1-mm-thick silicone polymer).[20] Although measurements of optical power with the HACR are generally performed with this heater, a second heater of completely different construction was also installed so as to permit tests of the temperature rise obtained for a different electrical heating configuration. This second heater is a resistive wire that is noninductively wound around the outside of the upper end of the cavity.

Superconducting niobium wires are used to provide electrical connections to the heaters. These wires are also thermally anchored to the cavity with thermally conductive varnish to avoid nonequivalence errors that could be caused by alternate pathways for heat to leak from the cavity.

5. Cavity Thermometry

As shown in Fig. 2, two GRT's are located within copper cylinders that are soldered to the inside of the top end cap of the cavity, one in the center and the other off center. Two thermometers were installed to allow for systematic checks (discussed in Subsec-

tion 3.C) and for insurance in the event of failure of one of the thermometers. The leads connected to each thermometer are wrapped around the copper cylinders and secured with conductive varnish.

6. *Optical Path*

The optical beam enters the radiometer through a window at the bottom of the cryostat, passes through apertures in the centers of two sets of large-area annular quadrant photodiodes, and enters the cavity through the aperture in its bottom end cap. The flange holding the window is machined so that the light is incident upon the window at the Brewster angle. By the use of light polarized in the plane of incidence of the window, the reflectivity of the window is minimized. The window flange is attached to the cryostat with a bellows and has three equally spaced screws that are adjusted to minimize the light reflected from the window. The 50-mm-diameter, 6-mm-thick window is made of high-quality fused silica.

To facilitate alignment of the laser light into the cavity and to measure the amount of laser light scattered out of the beam, two sets of four annular quadrant silicon photodiodes, each 50 mm in diameter with a 9-mm-diameter central aperture to pass the beam, are located along the optical path. One set is located at the bottom of the 77-K shield, and the other is located at the bottom of the 4.2-K shield. Each set consists of four independent quadrant photodiodes, which are operated in the photovoltaic mode. The photocurrent from each photodiode on the 77-K (4.2-K) shield is sent to a transimpedance amplifier with a gain of 10^7 (10^8) V/A. The apertures in the two sets of quadrant photodiodes are the limiting apertures in the optical path. The diameter of the apertures in the shields (at the locations where the photodiodes are mounted) is 12 mm. The distance from the quadrant photodiodes on the 4.2-K shield to the entrance of the cavity is 4 cm, and the distance between the sets is 22 cm.

For the entrance of scattered background light and thermal radiation into the cavity to be minimized, a radiation trap is located between the two sets of quadrant photodiodes. This trap consists of a tube of 1.5-mm-thick, 60-mm-diameter copper and two baffles within this tube. (The apertures in the baffles do not limit the field of view of the cavity.) The trap is attached to the 4.2-K shield and coated with a diffusely reflecting black paint.[17]

B. Laser System

A collimated beam of polarized light with a typical power level of 0.8 mW is required for high-accuracy measurements with the radiometer. In addition it is convenient, when silicon-photodiode transfer detectors are used, for the bandwidth of the light to be smaller than 0.01% of the wavelength. (Because the quantum efficiency of silicon photodiodes is nearly 100% in the visible, their spectral response increases roughly linearly with wavelength. Hence for these detectors to be calibrated with a relative standard uncertainty of 0.01%, either the wavelength must be known to 0.01% or the spectrum of a broad source must be well characterized; the former is more convenient.) Although this is not a rigid requirement, these considerations lead one to the use of laser sources.

The optical system for measurements at visible wavelengths is shown in Fig. 3. The primary goal of the optical system is to generate a geometrically well-defined optical beam with a power level stable to better than 0.01% over the time required for optical measurements. Power stability is accomplished by the use of a laser stablizer[21] with an external monitor photodiode that receives a reference beam from a reflection from a wedged window. The feedback loop in the stabilizer controls the power in the optical beam so as to maintain a constant signal at this reference photodiode. So that all possible sources of fluctuations in the power of the beam can be compensated by the feedback loop, the beam splitter is located as far downstream in the optical path as possible.

So that the reference photodiode is shielded from stray light, it is located inside a box with a small entrance aperture. Although the reference beam is first visually aligned into the aperture, it is useful to have a measurable signal to check the alignment. A convenient and sensitive test is to adjust the angle of reflection of the reference beam from the wedged window so as to *minimize* the signal on a test detector (located, for example, in the position of the trap detector in Fig. 3). Recall that if the reference beam is moved off of the reference photodiode, the stabilizer will increase the transmission so as to maintain a constant signal from this photodiode, thus resulting in an increase in the signal on the test detector. Hence when the signal on the test detector is minimized, the reference beam is optimally aligned onto the reference photodiode.

We obtain a well-defined beam by focusing the laser light with a microscope objective (focal length of 15 mm) on a 25-μm aperture. The microscope objective is slightly defocused to overfill the aperture, creating an Airy diffraction pattern. A variable iris was used to allow only the bright central spot of the diffraction pattern to pass through. Because the edges of the iris can be located at the first minimum

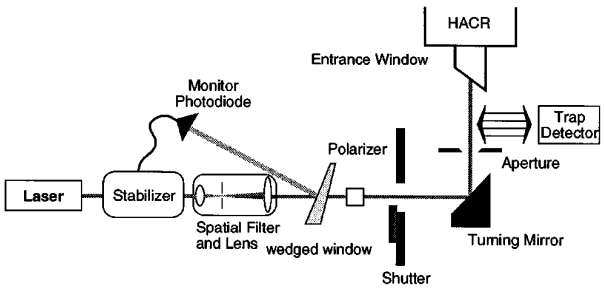

Fig. 3. Laser system for optical power measurements with the HACR.

of the diffraction pattern, there is minimal scattering from these edges. A recollimating lens is then located so as to yield a beam waist near or slightly beyond the cavity; the typical beam diameter is 1–2 mm. The location of the focal point of the lens is not critical; as a test, we located the waist before the Brewster window, thus producing a 6-mm-diameter diverging beam at the cavity, and we found less than a 0.03% change in the calibration of a trap detector (see Subsection 2.C.3.).

The only optical elements in the beam following the wedged window are a Glan–Thompson polarizer that is adjusted to minimize the reflection from the Brewster window and a mirror that reflects the laser light into the radiometer. The polarizer is located after the wedged window so that any possible birefringence in the wedge will not lead to imperfect linear polarization at the entrance to the radiometer. Because the laser light is nearly 100% polarized after exiting the stabilizer, there should not be any laser power instability generated by this arrangement. Although the final turning mirror could affect the polarization of the beam if the direction of the polarization were at an arbitrary angle to the plane of incidence, this effect is negligible in this system because the light is polarized perpendicular to the plane of incidence of the mirror. A computer-controlled shutter is positioned before the final turning mirror to block the laser during electrical heating of the cavity. For scattered laser light to be minimized, an aperture is located just above the turning mirror (but below the height at which transfer standards are rotated into position; see Subsection 2.C.3.). This aperture can typically reduce the signal on the quadrant photodiodes by a factor of 5.

C. Measurement Instrumentation

The measurement and control system is shown schematically in Fig. 4. The various subsystems are described below.

1. *Temperature Measurement*

Cavity temperature measurements are made by measurement of the resistance of the GRT's by the use of a standard four-wire configuration. A fixed current of 10 μA is supplied to the GRT by the use of a constant current source, and voltage V_{GRT} across the GRT is measured with a dedicated digital nanovoltmeter. The resistance of the cavity GRT varies from 780 Ω (at 5.0 K) to 580 Ω (at 5.8 K); hence the magnitude of V_{GRT} is between 7.8 and 5.8 mV. We determine V_{GRT} by averaging voltages $V_{\mathrm{GRT}+}$ and $V_{\mathrm{GRT}-}$, which we obtain by averaging four measurements that use positive and negative polarity of the applied current, respectively. This approach is used to eliminate voltage offsets from thermoelectric junctions in the wiring. A settling time of 10 s is allowed after the change in the polarity of the current before the GRT voltage is measured.

2. *Electric Power*

The electrical power applied to cavity heater P_H is given by $V_H I_H$, where V_H is the voltage across the heater and I_H is the current flowing through it. In terms of the actual measured quantities,

$$P_H = \frac{V_H V_R}{R}, \tag{1}$$

where V_R is the voltage across a standard resistor in

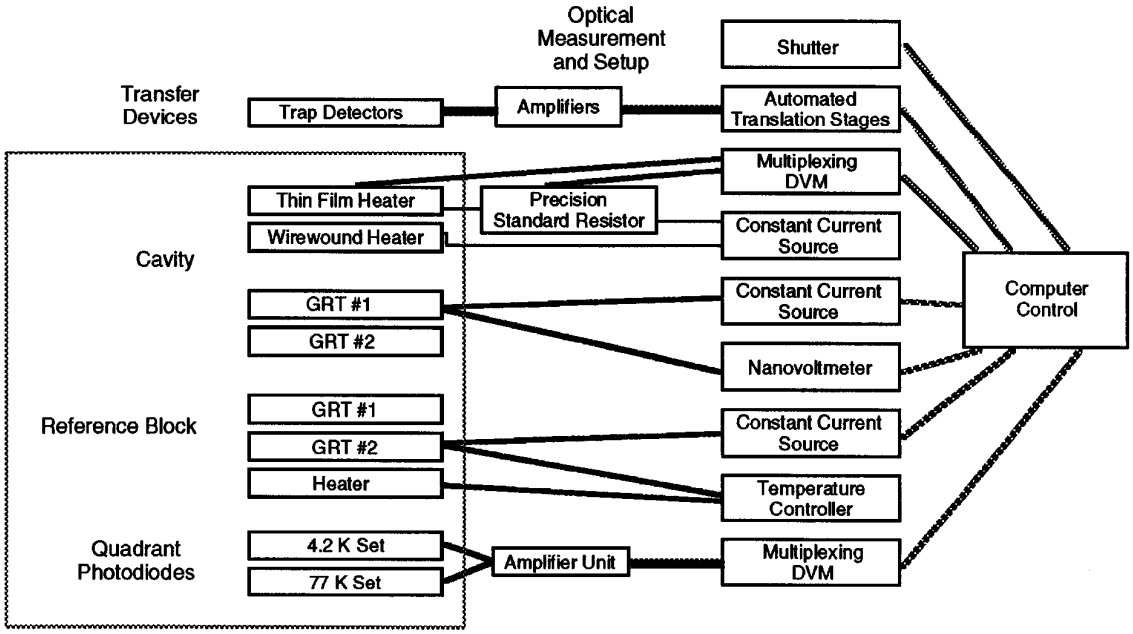

Fig. 4. Schematic diagram of the HACR measurement instrumentation. The elements shown within the box are inside the HACR Dewar.

series with the heater, and R is the resistance of the standard resistor (10.00079 kΩ). Using a standard four-wire dc measurement, one can measure V_H through a multiplexer with a high-accuracy digital voltmeter. The same voltmeter and multiplexer are also used to measure V_R. Current I_H is supplied by a constant current source.

The resistance of the thin-film heater decreases from 9700 Ω (at 5.0 K) to 8500 Ω (at 5.8 K). Because the current to the heater is held constant during a measurement, this dependence causes the actual electrical power dissipated in the heater to depend on its temperature. It would be preferable for the resistance to be independent of temperature. However, the negative heater temperature coefficient does produce a compensating or damping effect for thermal noise. If the temperature of the heater increases (for example, from temperature drift of the cavity), its resistance and hence the dissipated power decreases, which reduces the magnitude of the temperature excursion. This is preferable to a positive temperature coefficient, which would tend to magnify any temperature fluctuations.

3. *Transfer Standard Detectors*

Transfer standards must be used to transfer the optical power measurements with the HACR to other instrumentation used for radiometric measurements. Typically, silicon-photodiode light-trapping detectors[1,2,4] are used as high-accuracy transfer detectors in the visible and UV spectral ranges, whereas other solid-state detectors and thermal detectors (such as pyroelectric and thermopile detectors) are typically used at infrared wavelengths. Measurements of the quantum efficiency of trap detectors in the spectral range from 406 to 920 nm are described in a companion paper.[5] However, in Section 3 of this paper we describe measurements performed with these detectors that were useful for evaluating certain components of the measurement uncertainty of the HACR.

The transfer-standard detectors are mounted on a motor-driven rotating carousel, which positions the detectors in the optical beam path below the Brewster window. The carousel is mounted on a linear translation stage, which, with the rotation, permits alignment of each detector to the optical axis. The rotation and the linear translation are computer controlled, allowing for automatic alignment and repeatable positioning of the transfer-standard detectors. Signals from the trap detectors are measured with calibrated transimpedance amplifiers and a multiplexing digital voltmeter.

D. Thermal Characterization

We facilitate determination of the approximate heater current required to produce a given equilibrium voltage on the cavity GRT during a measurement cycle by first characterizing this relationship in advance, and then, during the course of operation, improving the baseline characterization iteratively. This baseline measurement relates the equilibrium cavity GRT voltage V_E to the programmed value of the electrical heater current I_H rather than to the heater's corresponding input power. When I_H is changed, sequential determination of V_{GRT} shows convergence toward a new equilibrium value. We tested the thermal behavior of the cavity by stepping I_H through the normal range of input currents, in both increasing and decreasing passes, and finding V_E at each setting.

We determined the equilibrium cavity GRT voltage V_E by fitting V_{GRT} as a function of time to a double exponential function, as shown in Fig. 5. This empirically determined functional form was found to converge to the same equilibrium value, within fitting uncertainty, regardless of the previous cavity temperature. Other functional forms, such as a single exponential, yielded a bias in the predicted equilibrium values depending on whether the temperature was increasing or decreasing toward the new equilibrium. (An analysis of the thermal characteristics of the system will be presented in an upcoming paper.) The temporal behavior of V_{GRT} after a step change in I_H is described by

$$V_{\mathrm{GRT}} = C_0 + C_1 \exp(-t/\tau_1) + C_2 \exp(-t/\tau_2), \quad (2)$$

where $\tau_1 = 116 \pm 3$ s and $\tau_2 = 245 \pm 8$ s. The values of τ_1 and τ_2 were determined by nonlinear least-squares fits to 21 data series. The uncertainties given are the standard deviations of the values obtained from these fits. This expression (with τ_1 and τ_2 held fixed) allows coefficients C_0, C_1, and C_2 to be determined by linear fitting in real time, in a closed-form expression that is computed quickly after each new determination of V_{GRT}. The accuracy with which these fitting parameters can be determined is insensitive to the exact values of τ_1 and τ_2. When the relative standard uncertainty in the value of fitting parameter C_0 drops below 10^{-5},

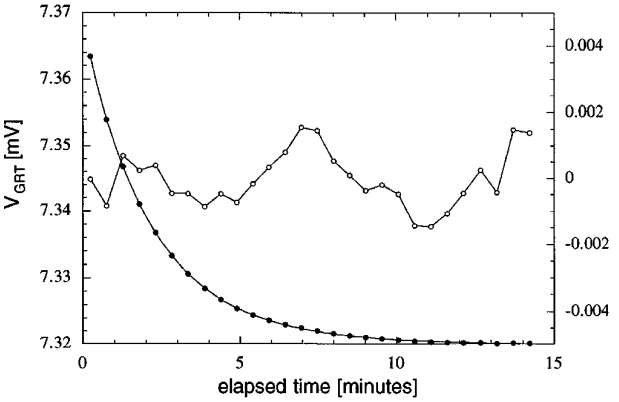

Fig. 5. Plot illustrating the time dependence of cavity GRT voltage V_{GRT} for heat input. The data shown by filled circles were fit to a double exponential form (shown by the solid curve) as described in the text. The open circles show the percentage deviation of the data from the fit. The scale for the data is on the left-hand y axis, and the scale for the percent residuals is on the right-hand y axis.

V_E is assigned the value of C_0. This process is usually completed within 15 min, or roughly four times the longest time constant.

We determined a functional form $V_E = F(I_H)$ by fitting the data for V_E versus I_H to a fifth-order polynomial. This function was then inverted numerically and fit by a new polynomial function $I_H = G(V_E)$, which is shown in Fig. 6. This function is used to estimate the current needed to produce a given equilibrium GRT voltage.

To understand the shape of $G(V_E)$, we applied the basic heat-conduction law in conjunction with the temperature dependences of the GRT resistance, heater resistance, and conductance of the thermal link. We used a standard functional form[22] to fit calibration data for the cavity GRT, an estimate for the temperature dependence of the conductance of the thermal link, and a fit to data for the temperature dependence of the heater resistance. The calculated shape of $G(V_E)$ is also shown in Fig. 6, and it is in excellent agreement with actual function $G(V_E)$. The only adjustable parameter was the conductance of the thermal link at one temperature, which was varied so as to overlap the calculated shape with $G(V_E)$. $G(V_E)$ is remarkably linear, which would not necessarily be expected beforehand. Because the required heater power varies linearly with the temperature change of the cavity (neglecting the temperature dependence of the conductance of the thermal link), the heater current varies as the square root of the temperature change (neglecting the temperature dependence of the heater resistance). However, because of the compensating nonlinear dependence of the GRT resistance on temperature, the dependence of I_H on V_E is roughly linear. The shape of $G(V_E)$ is only weakly dependent on the temperature dependences of the heater resistance and thermal link conductance.

In principle, the reference-block temperature is fixed, and the temperature of the receiving cavity depends solely on the applied power (either optical or electrical). In practice, the cavity temperature drifts on a time scale of many hours. We believe that this slow drift is due to changes in the temperatures of the Brewster window and thermal shields. As a way to correct for these small drifts, an additional parameter ΔI_H was used to adjust the predicted heater current. This small adjustment to the heater current is determined during each measurement cycle and is given by

$$\Delta I_H = (V_L - V_1)\frac{dI_H}{dV_E}, \tag{3}$$

where V_L is the equilibrium GRT voltage obtained from optical heating and used to determine I_H, and V_1 is the actual equilibrium GRT voltage obtained from the application of a current of I_H to the heater. The derivative of function $G(V_E)$ is evaluated from the coefficients of a fifth-order polynomial. The value of ΔI_H is used and then updated each measurement cycle.

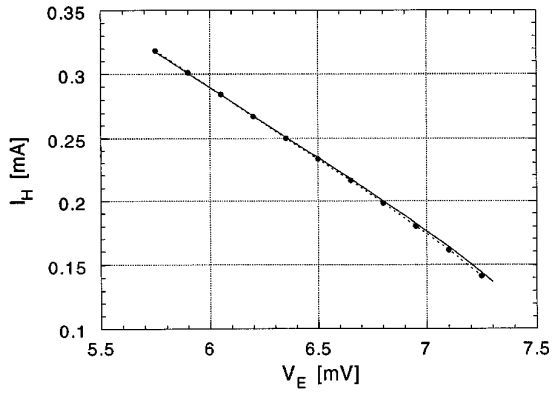

Fig. 6. Function $G(V_E)$ that is used to predict heater current I_H needed to produce a given equilibrium GRT voltage. The solid curve shows $G(V_E)$, and the dotted curve (with filled circles) shows a calculation of the expected shape of $G(V_E)$ as described in the text.

3. Optical Power Measurements

A. Measurement Procedure

Because of the 4-min time constant of the cavity, measurements of optical power with the HACR are very time consuming. Initial measurements were made manually; an operator watched the time behavior of the cavity GRT voltage (sampled every 60 s), along with a running average of ten measurements. When the apparent equilibrium temperature was reached, the value of the running average was recorded. Experience showed that this required 30 min or more. To reduce both the subjective judgment and the time and human resources for the measurements, we developed the exponential fitting algorithm (described above) that yields a reliable prediction of the equilibrium GRT voltage in approximately 15 min. Furthermore, the entire measurement procedure is computer controlled, allowing for unattended operation. We now discuss the measurement algorithm.

The measurement of optical power using the HACR requires the determination of the electrical power required to produce the same equilibrium cavity GRT voltage V_L as was produced under the influence of optical heating. This is accomplished in three cavity-temperature measurement cycles, the first with laser heating of the cavity followed by two iterations with applied electrical power. Thus one complete measurement of laser power is completed in approximately 45 min.

The measurement sequence is initiated when the shutter is opened, which begins the optical heating cycle. After V_L has been determined, the shutter is closed and electrical heating begins. A first estimate of the heater current that is expected to reproduce V_L (determined from the thermal characterization described in) is applied to the heater. The equilibrium GRT voltage V_1 and its corresponding heater power P_1 are then measured. From the difference between V_L and V_1, a small correction ΔI_H

is applied and a new value for the heater current is determined. This new value of the heater current is applied and the new equilibrium GRT voltage V_2 and its corresponding heater power P_2 are measured. The value of electrical power P_H that would produce V_L is then calculated with a linear approximation, given by

$$P_H = \frac{P_1(V_2 - V_L) + P_2(V_L - V_1)}{V_2 - V_1}. \quad (4)$$

Optical power P_L is then given by

$$P_L = \frac{1}{T}\left(\frac{NP_H}{A} + P_S\right), \quad (5)$$

where P_S is the estimated optical power scattered out of the field of view of the cavity, A is the absorptance of the cavity, T is the transmittance of the entrance window of the HACR, and N is a factor to take into account any nonequivalence between the optical and electrical heating. We discuss the measurement and uncertainties of these corrections in the next subsection.

Concurrent with the first electrical heating cycle, the response of the transfer detectors is measured. During the first electrical heating cycle, the transfer-standard detectors are sequentially rotated in front of the window, and the shutter is opened. The signals from the transfer detectors are measured both with the shutter open and closed to correct for offsets caused by background or scattered light.

B. Corrections and Type B Uncertainties

The components of the 0.021% combined relative standard uncertainty in a measurement of P_L are listed in Table 1. (Hereafter the combined relative standard uncertainty is referred to by the shortened phrase combined uncertainty, and the relative standard uncertainty components are referred to by the shortened phrase uncertainty components.) They are divided into components arising from type B (0.019%) and type A (0.010%) uncertainties.[23] (The terms type A and type B distinguish between uncertainties that are determined by statistical methods or other methods, respectively.) The type A component is discussed in Subsection 3.D. The largest correction factor and associated uncertainty component is in the measured value of the transmission of the entrance window (T). Other corrections include the measured values of scattered optical radiation (P_S) and the cavity absorptance (A). Also listed is the uncertainty component in the value of N, which is based on experimental tests for possible nonequivalence errors, described in Subsection 3.C. (No correction is applied for nonequivalence; hence $N = 1$.) The uncertainty component in P_H consists of the small uncertainties in the measurements of V_H, V_R, and R. The value of R was obtained from a direct calibration at NIST, whereas the voltage measurements are traceable to NIST through the manufacturer of the digital voltmeter.

With the single exception of P_S, the components of the combined relative uncertainty in P_L are approximately equal to the relative uncertainties in the measured quantities themselves; this is because T and A are very nearly equal to unity, and $P_S \ll P_H$. For P_S the relative uncertainty component is obtained by multiplication of the relative uncertainty by the ratio of P_S to P_H. We now discuss the most important of these uncertainties in more detail.

1. *Window Transmission*

A correction is applied to the optical power measurement to account for the transmittance of the entrance window. The transmittance is determined when the signal on a silicon-photodiode trap detector is measured with and without the window in the beam. These measurements are performed with the window removed from the HACR. The window is oriented at the Brewster angle by minimization of the reflection, which is the same method used when the window is installed in the HACR. Minimizing the reflection is not a critical adjustment and can be done by eye (or at near-infrared wavelengths, with an infrared viewer).

Cleanliness of the window, as well as careful measurements of its transmittance, are required to minimize the correction and uncertainty. To arrive at a typical value for the window transmittance and its uncertainty, we use the results of a recent series of measurements at nine wavelengths between 406 and 920 nm. For each wavelength, the window transmittance was measured before it was installed in the HACR. The measurements were repeated many times with a new alignment of the Brewster angle and position of the beam on the window. For these nine wavelengths, the mean transmittance measured on clean windows that were ready for installation in the HACR was 0.99976. The typical relative standard deviation of these measurements at any given wavelength was 0.01%, caused by a combination of measurement uncertainty and spatial variation. A window was typically installed in the HACR for a few days to a few weeks, while optical power measurements were carried out. The window was then removed and the transmittance measured again. The mean transmittance after removal was 0.99963, and the typical relative standard deviation at any given wavelength was 0.016%; the increased relative standard deviation was due to increased spatial variation across the window. This drop in transmission and increased spatial variation was reversible upon cleaning the window and is presumed to be due to contaminants that were deposited on the window. Because we do not know exactly when these contaminants collected on the window, or exactly what region of the window the beam passes through during the optical power measurements, we must assign an uncertainty that encompasses the full range of the transmittance values obtained. For each wavelength we determined the correction to the optical power by averag-

ing all the transmittance values obtained (before and after), and we assumed a uniform probability distribution for all these values to assign the uncertainty. The transmittance correction and associated uncertainty component quoted in Table 1 is the average transmittance (0.99970) and average uncertainty (0.016%) for the nine wavelengths at which we have made measurements. The uncertainty of the window transmittance dominates the total uncertainty for optical power measurements with the HACR, and we could obtain improved accuracy by reducing this uncertainty. We expect that the uncertainty in the window transmittance can be reduced to below 0.005% with improved methods for the measurement and cleaner conditions in the laboratory.

Although one side of the window is under vacuum during HACR operation, the window transmittance measurements are performed in air. The pressure drop across the window could, in principle, affect the reflectance, if the window were stressed. However, we measured the reflectivity of the window while it was mounted on the HACR and found it to be less than 0.001% (this test was done at 770 nm). Furthermore, because the dominant cause of imperfect window transmittance appeared to be from contaminants on the window, we expect no increase in the uncertainty in this correction caused by this issue.

2. *Scattered Optical Power*

Light can be scattered at small angles by elements in the optical system such that it is still near the beam upon entrance to the HACR but does not enter the cavity. A correction is applied to the optical power measurement for this scattered laser light. (This light would also be intercepted by the trap detectors.) Because most of this light is still near the beam, we account for it by summing the optical power detected by the eight quadrant photodiodes and by using this value for P_S in Eq. (5). For an optical power level of 0.8 mW, the typical magnitude of P_S is 50 nW. Light can also be scattered by the Brewster window, and some may be scattered outside the cone that will impinge on the quadrant photodiodes. However, light scattered into large angles will tend to be accounted for in window transmittance measurements. There is a range of angles for which light scattered by the window does not reach the trap detector used during transmittance measurements, but that does reach the quadrant photodiodes. The optical power associated with this light is accounted for twice (in both the transmittance and scattered power corrections) and thus constitutes a systematic error. Hence we have assigned a conservative uncertainty component that is equal to P_S/P_H. Ideally, the trap detector used during transmittance measurements should be located such that its active area subtends the same solid angle as is subtended by the quadrant photodiodes, with the center of the window as the origin in both cases.

To investigate the issue of scattered laser light further, we simulated the trajectory of the beam outside the HACR (but with a Brewster window in the beam path) so that we could measure the variation in the optical power along the beam path. Similar measurements were recently discussed by Stock *et al.*[19] We found that the signal on a trap detector that was translated by 65 cm (corresponding to the distance between the carousel and the HACR cavity) varied by less than 0.01%, which is consistent with the magnitude of the optical power detected by the quadrant photodiodes. We also found that the aperture located just after the last turning mirror affected the level of variation in the optical power along the beam path, which is consistent with our observation that this aperture reduces significantly the signal on the quadrant photodiodes.

Table 1. Components of the Combined Relative Standard Uncertainty of 0.021% in the Measurement of Optical Power by the HACR[a]

Type	Typical Value of Correction	Component of Uncertainty (%)
Type A		0.010
Type B, combined		0.019
Window transmittance (T)	0.99970	0.016
Scattered optical power (P_S), nW	50	0.006
Cavity absorptance (A)	0.99998	0.002
Nonequivalence (N)	1.00000	
Power dependent		0.005
Temperature gradients		0.004
Heater power (P_H)		
V_H, V_R		0.003
R		0.0003

[a]The optical power level is 0.8 mW. The type A uncertainty at other power levels is shown in Fig. 9. The measured value of A and representative values of T and P_S are also listed.

C. Nonequivalence Errors

The underlying principle of electrical-substitution radiometry is the equivalence of optical and electrical heating, i.e., the requirement that a given quantity of power absorbed by the cavity will lead to a certain temperature rise, regardless of whether the source of this power is the electrical heater or incident laser light. Potential sources of nonequivalence require calculated estimates or indirect systematic checks to establish their magnitude.

Nonequivalence errors were considered by Quinn and Martin[10] and by Martin *et al.*[12] Because the design of the HACR closely parallels the radiometer described by Martin *et al.*,[12] much of the analysis in this study is relevant to the HACR. However, there are also nonequivalence issues associated with the differences between the HACR and the Martin *et al.* radiometer. We present additional systematic checks that we performed to test for possible nonequivalence errors. In the context of our automation sequence, we use the term nonequivalence to refer to any difference between the response of the HACR for the optical and electrical heating cycles, even when the cause is not actually a difference in optical and electrical heating. This distinction will become clearer in the subsequent discussion.

1. Power-Dependent Nonequivalence Errors

The actual observable used to compare optical and electrical heating is the voltage across the GRT that is thermally sunk to the cavity. Although background heat sources that could elevate the cavity temperature above that of the reference block (or the GRT temperature above that of the cavity) are minimized, any remaining background heat sources must have the same magnitude for both the optical and electrical heating cycles. Here background includes all sources other than optical or electrical heating; an example is self-heating of the GRT.

To test for a nonequivalence caused by different background levels, one can measure the quantum efficiency of a detector known to be linear[13] as a function of laser power. Any difference in background will result in a systematic dependence of the measured quantum efficiency η_m on the measured optical power P_m. We performed such an experiment with silicon-photodiode light-trapping detectors; the results are shown in Fig. 7 for two cases: before (shown by open circles) and after (filled squares) a nonequivalence in background heating was eliminated. If we suppose that the origin of the systematic dependence shown by the open circle data in Fig. 7 is due to a nonequivalence in background heating, then this dependence can be modeled by

$$\eta_m = \eta \frac{P_m - C}{P_m}, \tag{6}$$

when η and C are fitting parameters that represent the true quantum efficiency and the difference in background heat, respectively. As shown in Fig. 7, the data shown by open circles are well fit with $\eta = 0.99602 \pm 0.00002$ and $C = 153 \pm 19$ nW. The excellent quality of the fit supports the analysis.

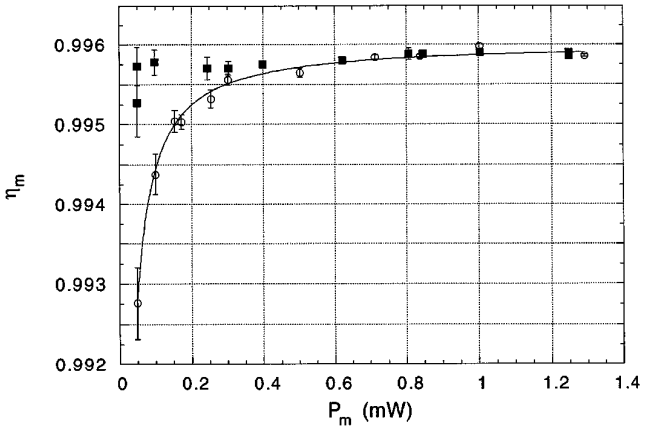

Fig. 7. Plot illustrating how a nonequivalence in background heat can lead to a dependence of the measured quantum efficiency of a trap detector η_m on the measured optical power P_m. The open circles (filled squares) show data taken before (after) a nonequivalence in background heating was eliminated. The solid curve shows the result of fitting the data shown by open circles to Eq. (6). At low values of P_m, where the type A uncertainty dominates, the error bars represent the standard deviation of the mean.

This would result in a 0.019% nonequivalence error for a laser power of 0.8 mW. For the data shown by filled squares, the fit yeilds $C = 24 \pm 10$ nW, which puts an upper limit of 0.003% for this source of nonequivalence.

The background heat difference was rooted in an electrical transient that was produced by the current source for the cavity GRT when the sign of the current was reversed. Such a heat source, if constant, would not lead to a nonequivalence; however, the nonequivalence arose because of a slight difference in the rate of current reversals between the optical and electrical cycles. This difference was due to the integration of trap-detector measurements into the first electrical cycle. We easily eliminated the transient by briefly switching the current off before changing its sign.

Measuring the variation of a quantum efficiency calibration with optical power actually tests for any source of nonequivalence that is dependent on the optical power. The data obtained after elimination of the extraneous heat source, shown as filled squares in Fig. 7, were used to put an upper limit on the magnitude of any such nonequivalence error. This required choosing the expected systematic dependence and fitting the data to that form. To derive an approximate upper limit for power-dependent nonequivalence errors (without knowing the expected form), we fit the data shown by filled squares in Fig. 7 to a line and use half of the change in quantum efficiency from zero laser power to 1 mW. This approximate upper limit is 0.003 ± 0.002%, whereas for the data using another trap detector (not shown) it was 0.007 ± 0.002%. From these tests we estimate a contribution of 0.005% to the uncertainty in the value of N.

2. Cavity-Temperature Gradients

The temperature rise induced at the location of the cavity GRT must be independent of the heating source. Hence the cavity GRT is located near the thermal link, which is a region through which all the heat conducted through the thermal link must flow, regardless of the heating source. One can obtain additional insurance by making the location of the optical heating similar to that of the electrical heating. Because the thin-film heater is located where the laser beam is incident upon the inclined surface of the cavity, heat is deposited from both the laser light and the electrical heater at nearly the same location. In addition, the increased radiation from any area that potentially could be overheated (i.e., not remain in thermal equilibrium with the cavity) would be predominantly reabsorbed in the cavity itself. Nevertheless, it is desirable to have some test of these issues. We have performed one test and plan to do a second test in the future. To test whether there might be a nonequivalence in the temperature rise induced at the location of the GRT, we measured the quantum efficiencies of four trap detectors by using a second GRT that is located off

center on the top of the cavity. The average difference in the quantum efficiencies that were measured with this GRT, as compared with those that were measured with the centered GRT, was $-0.002 \pm 0.004\%$. The second test is to compare the results obtained with the wire-wound heater with those obtained with the thin-film heater. Unfortunately, failure of the connections to the wire-wound heater has delayed such a test. Nevertheless, this test was described by Martin *et al.*[12] using two wire-wound heaters; the result found was that the temperature rise of the cavity, as measured by a GRT in the same location as the central GRT on the HACR, was independent of the heater used to within 0.002%. We expect that the thin-film heater should mimic the heating produced by the laser even more closely than does a wire-wound heater. Based on these two tests and the results of Ref. 12, we estimate a contribution of 0.004% to the uncertainty in N.

D. Type A Uncertainties

To evaluate the precision of the HACR, we want to repeat measurements of the optical power and evaluate the standard deviation in the measurements. However, this method presumes that the long-term drift of the optical power of the source is small compared with the typical random variation between sequential measurements. Drifts of the optical power that are slow compared with the time scale of an individual measurement of optical power by the HACR will not substantially affect the precision of any given measurement, but they will enlarge the standard deviation of a series of measurements. To address this issue, we recall that the HACR is used to calibrate transfer standards, and that the calibration factor will be approximately independent of slow drifts in the optical power of the source. Hence we evaluated the type A uncertainty of the optical power measurement by the HACR not by measuring the standard deviation of repeated measurements of the optical power, but rather by repeated determinations of the quantum efficiency of a trap detector. Implicit in this approach is that the random variations in the measured values of the quantum efficiency are dominated by the random variations in the determination of the optical power by the HACR. Figure 8 shows that this assumption, although not perfect, is reasonable. (For this particular data set the long-term drift of the laser power was very small.) Using a He–Ne laser as the source, we found that the relative standard deviation of a series of repeated measurements of the quantum efficiency was typically 0.010% at an optical power level of 0.8 mW. This value is listed in Table 1 as the type A component of uncertainty.

Further insight into the sources of this type A uncertainty was obtained by examination of its variation with optical power. (Once again, we assume that the random variations in the determination of quantum efficiency are dominated by the HACR measurement.) Because of our study of power-dependent nonequivalence errors (Subsection 3.C.1.), these data were readily available to us and are shown in Fig. 9. The data are well fit by the assumption that the relative standard uncertainty varies inversely with the optical power. Neglecting variation in the conductance of the thermal link, we would expect this for a system that is dominated by an absolute uncertainty in temperature measurement that is independent of optical power. We now describe a series of experiments that support this hypothesis. Each experiment can be viewed as a progressive decrease in the complexity of the HACR measurement.

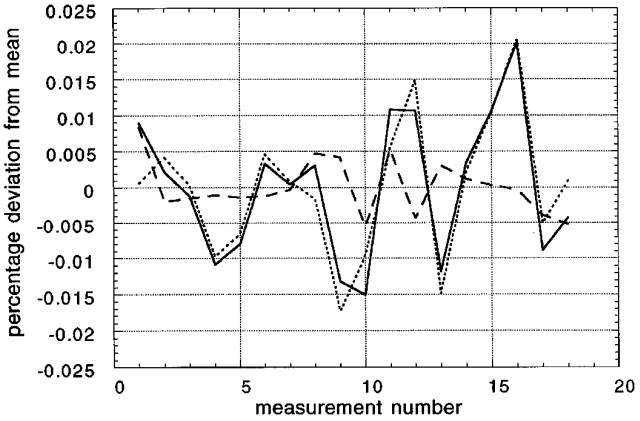

Fig. 8. Plot illustrating the variations in repeated measurements of three quantities: the optical power of an intensity-stabilized He–Ne laser as determined by the HACR (solid curve), the signal from a trap detector illuminated by this laser (dashed curve), and the quantum efficiency of the trap detector as determined from the first two quantities (dotted curve). We can see that the dominant source of random variation in the measurement of quantum efficiency is in the optical power measurement by the HACR.

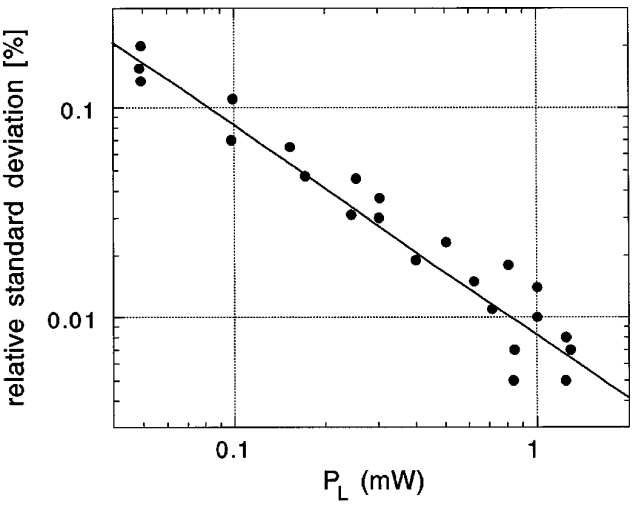

Fig. 9. Type A uncertainty of the HACR versus optical power, as measured by the relative standard deviation in measurements of the quantum efficiency of a trap detector. The solid curve shows a fit of the data to a form that varies inversely with optical power.

1. *High-Accuracy Cryogenic Radiometer Measurements of the Electrical Heater Power*

The first experiment simply was to use an electrical heating cycle in place of the usual optical cycle. Because the electrical power from the heater is quite stable (the drift of the heater power in an overnight run was typically 0.003%), we can directly evaluate the precision of a HACR measurement of electrical heating. This experiment allows us to eliminate optical contributions to the uncertainty, in particular the contribution of the laser stability. (Here we are interested in the stability of the optical power for the 15 min of the optical heating cycle, rather than the long-term stability.) We found that the standard deviation of repeated measurements of the electrical heater power was 0.008% at a power of 0.8 mW, which roughly indicates the magnitude of the optical contributions to the 0.010% standard deviation. In tests of the stability of the He–Ne laser, which we performed by monitoring the signal on a trap detector placed in the beam, the maximum observed change in the signal in 15 min was 0.005%.

Because we knew the actual power of the electrical heater from the measurements of V_H, V_R, and R, we compared this value with the result obtained from the HACR. In our first tests, we found a reproducible difference of $-0.008 \pm 0.004\%$ between the actual heater power and the HACR's determination of the heater power. This percentage difference was independent of the heater power; hence this systematic error was not apparent in our tests for power-dependent nonequivalence errors. The discrepancy was traced to a small transient that injected power into the heater circuit when the multiplexing digital voltmeter read the signal from the transimpedance amplifiers that are used with the trap detectors. (This multimeter is used with a multiplexing unit, which allows one meter to be used for trap-detector amplifier output voltage, heater voltage, and standard resistor voltage measurements, but unfortunately also allowed for coupling of the amplifier circuits to the heater.) Upon eliminating this problem, we found that the actual heater power agreed with the HACR's determination of the heater power to within 0.001%.

2. *Stability of the Cavity-Temperature Measurement*

We then simplified the computer control further by not varying the heater current, as it normally would be in the two electrical heating cycles (see Subsection 3.A). This allowed us to observe the repeatability of V_E for a fixed heater current. Random variations in V_E that occur in the absence of any change in the applied heater power are measurement errors that will result in uncertainty in all HACR measurements. The magnitude of this uncertainty was determined by the use of the function $G(V_E)$ to determine the variation in heater current (and hence heater power) that would result from the observed variation in cavity GRT voltage. We found that the standard deviation in either $V_L - V_1$ or $V_L - V_2$ was typically 90 nV, which corresponds to a 0.006% variation in the heater power for an applied heater power at 0.8 mW. Hence the repeatability of V_E accounts for most of the observed standard deviation of 0.008% described above.

Two possible sources of the observed cavity GRT temperature variations are instability of the reference-block temperature, and temperature variations induced in the cavity by the cavity GRT measurement instrumentation. In addition, there may be purely electronic noise (i.e., not caused by real temperature changes) on the cavity GRT voltage. To investigate these issues and improve the thermal performance of the HACR, we are currently testing the use of ac bridge electronics for both the cavity GRT resistance measurement and the reference-block GRT control sensor.

Another source of variation in the cavity temperature is a change in the thermal radiation from the Brewster window. In Ref. 12 it was estimated that for the geometry of this radiometer, 13 μW of the power emitted by the window is absorbed by the cavity. Drift in the window temperature affects the cavity temperature, but only drifts on the time scale of a HACR measurement lead to an error in the HACR measurement of optical power. (Note that this contribution to the uncertainty budget has already been included in the tests of the cavity-temperature stability discussed above.) Although the window temperature may drift by 0.5 to 1.0 K as the laboratory changes temperature, we estimate that only rarely will the window temperature change by more than 0.1 K on the time scale of a HACR measurement. A 0.1-K change in the window temperature would lead to a 0.13% change in the thermal radiation from the window, which, for the above 13-μW estimate, is only 0.002% of our typical 0.8-mW optical power. We tested the effect of drift in the window temperature experimentally by heating the entire window flange by a few degrees with a heating tape, while monitoring both the flange temperature (as close to the window as possible) and the cavity temperature. With this simple arrangement only a rough test could be performed, but our results were consistent with the expected temperature rise of the cavity, within 50%. Hence we are confident that the magnitude of this small (but not negligible) effect is understood.

4. Conclusion

We have described the construction and operation of the new NIST primary standard for optical power measurements, the high-accuracy cryogenic radiometer. A computer-controlled, automated measurement procedure has improved both the efficiency of optical power measurements and the evaluation of uncertainties. A detailed analysis of the uncertainty components has yielded a value of 0.021% for the combined relative standard uncertainty in the measurement of optical power, at an optical power of 0.8 mW. The dominant uncertainty component

(0.019%) arises from the uncertainty in knowing the actual window transmittance during a measurement. Systematic tests allowed us to detect and eliminate sources of nonequivalence that were not related to the thermal characteristics of the radiometer, but rather rooted in the instrumentation and the measurement algorithm. Such tests underscore the need for constant evaluation of potential systematic errors by as many methods as possible.

The uncertainty in optical power measurements with the HACR represent a fivefold improvement over the previous primary standard, a 100% quantum efficient device. In addition, the HACR can be used over a much larger range of wavelengths. In a companion paper, the realization of a new scale of absolute spectral response between 406 and 920 nm, based on the HACR, will be presented. We are currently extending the use of the HACR to ultraviolet and infrared wavelengths. A scheme for obtaining a wide tunable range from a single-laser system is being investigated.[24] At deep-ultraviolet wavelengths, the fundamental assumption that all the optical power is converted to heat will have to be revisited.

The analysis of uncertainties has revealed areas for future improvements of the HACR. Careful attention and procedures are required to determine accurately the value of the window transmittance. Alternatively, a system for eliminating this uncertainty can be implemented.[19] At the operating power of 0.8 mW that can be used at visible wavelengths, the type A uncertainty is approximately half of the combined type B uncertainty. However, significantly lower optical power may be required for transfer standards in other wavelength regimes, in which case the type A uncertainty will dominate. A series of measurements could then be averaged to reduce this uncertainty, if this is not precluded by drifts in the laser source or the transfer detector. Because improved temperature stability is required to reduce the type A uncertainty, we are currently investigating the use of ac bridge electronics for both the cavity GRT resistance measurement and the reference-block GRT control sensor.

We thank J. Fowler for his efforts in the construction and development of the HACR and in instrumentation issues. We thank D. Dummer and S. Lorentz for their contributions and interest in the HACR, and N. Fox for useful communications.

References and Notes

1. E. F. Zalewski and C. R. Duda, "Silicon photodiode device with 100% external quantum efficiency," Appl. Opt. **22,** 2867–2873 (1983).
2. C. L. Cromer, "A new spectral response calibration method using a silicon photodiode trap detector," presented at the 1991 Measurement Science Conference, Anaheim, Calif., 31 January–1 February 1991.
3. C. L. Cromer, G. Eppeldauer, J. E. Hardis, T. C. Larason, and A. C. Parr, "National Institute of Standards and Technology detector-based photometric scale," Appl. Opt. **32,** 2936–2948 (1993).
4. J. M. Houston, C. L. Cromer, J. E. Hardis, and T. C. Larason, "Comparison of the NIST high accuracy cryogenic radiometer and the NIST scale of detector spectral response," Metrologia **30,** 285–290 (1993).
5. T. R. Gentile, J. M. Houston, and C. L. Cromer, "Realization of a scale of absolute spectral response using the NIST high accuracy cryogenic radiometer," submitted to Appl. Opt.
6. F. Hengstberger, *Absolute Radiometery* (Academic, San Diego, Calif., 1989), Chap. 1, p. 30; Chap 6, p. 206.
7. D. C. Ginnings and M. L. Reilly, "Calorimetric measurement of thermodynamic temperatures above 0 °C using total blackbody radiation," in *Temperature:* Its Measurement and Control in Science and Industry, H. H. Plumb, ed. (Instrument Society of America, Pittsburgh, Pa., 1972), Vol. 4, Part I, pp. 339–348.
8. C. R. Yokley, "A radiometric calibration facility for low temperature blackbodies," Earth Resources Aircraft Program Rep. (NASA, Washington, D.C., 1976).
9. C. R. Yokley, "Long wave infrared testing at NBS," in *Applications of Optical Metrology: Techniques and Measurements II,* R. C. Harney, ed., Proc. Soc. Photo-Opt. Instrum. Eng. **416,** 2–8 (1983).
10. T. J. Quinn and J. E. Martin, "A radiometric determination of the Stefan-Boltzmann constant," in *Precision Measurement and Fundamental Constants II,* Natl. Bur. Stand. (U.S.) Spec. Publ. **617,** 291–297 (1984).
11. T. J. Quinn and J. E. Martin, "A radiometric determination of the Stefan-Boltzmann constant and thermodynamic temperatures between −40 °C and +100 °C," Philos. Trans. R. Soc. London Ser. A **316,** 85–189 (1985).
12. J. E. Martin, N. P. Fox, and P. J. Key, "A cryogenic radiometer for absolute radiometric measurements," Metrologia **21,** 147–155 (1985).
13. Fu Lei and J. Fischer, "Characterization of photodiodes in the UV and visible spectral region based on cryogenic radiometry," Metrologia **30,** 297–303 (1993).
14. Certain trade names and company products are mentioned in the text or identified in an illustration in order to specify adequately the experimental procedure and equipment used. In no case does such identification imply recommendation or endorsement by the National Institute of Standards and Technology, nor does it imply that the products are necessarily the best available for the purpose.
15. Model ITC-4, Oxford Instruments, Inc., 130A Baker Ave., Concord Mass. 01742.
16. Chemglaze Z302, Lord Corporation, Industrial Coatings Division, 200 West Grandview Blvd., Erie, Pa. 16514-0038.
17. 3M-Nextel, Minnesota Mining and Manufacturing, St. Paul, Minn. 55144-1000.
18. R. U. Datla, K. Stock, A. C. Parr, C. C. Hoyt, P. J. Miller, and P. V. Foukal, "Characterization of an absolute cryogenic radiometer as a standard detector for radiant-power measurements," Appl. Opt. **31,** 7219–7225 (1992).
19. K. D. Stock and H. Hofer, "Present state of the PTB primary standard for radiant power based on cryogenic radiometry," Metrologia **30,** 291–296 (1993).
20. M. Woolfrey, Oxford Instruments, Old Station Way, Eynsham, Witney, Oxon, U.K. (personal communication), 1995.
21. Model LS-100, Cambridge Research and Instrumentation, Inc., 21 Erie St., Cambridge, Mass. 02139.
22. G. K. White, *Experimental Techniques in Low Temperature Physics* (Oxford Univ., New York, 1987), p. 111.
23. B. N. Taylor and C. E. Kuyatt, "Guidelines for evaluating and expressing the uncertainty of NIST measurement results," NIST Tech. Note 1297, 2nd ed. (National Institute of Standards and Technology, Gaithersburg, Md., 1994).
24. T. R. Gentile and C. L. Cromer, "Mode-locked lasers for high accuracy cryogenic radiometry," Metrologia (to be published).